SOIL Discussions

Open Access

EGU

Monitoring soil salinity using time-lapse electromagnetic conductivity imaging

Maria Catarina Paz [1,2], Mohammad Farzamian [1,3], Ana Marta Paz [3], Nádia Luísa Castanheira [3], Maria Conceição Gonçalves [3], Fernando Monteiro Santos [1]

5 [1] Instituto Dom Luiz, Faculdade de Ciências da Universidade de Lisboa, Campo Grande, Edifício C1, Piso 1, 1749-016 Lisboa, Portugal

[2] CIQuiBio, Barreiro School of Technology, Polytechnic Institute of Setúbal, Rua Américo da Silva Marinho, 2839-001 Lavradio, Portugal

[3] Instituto Nacional de Investigação Agrária e Veterinária, Avenida da República, Quinta do Marquês (edifício sede), 2780-157 Oeiras, Portugal

10

Correspondence to: Mohammad Farzamian (mohammad.farzamian@iniav.pt)

Abstract

Lezíria Grande of Vila Franca de Xira, located in Portugal, is an important agricultural system where soil faces the risk of
salinization, being thus prone to desertification and land abandonment. Soil salinity can be assessed over large areas by the
following rationale: (1) use of electromagnetic induction (EMI) to measure the soil apparent electrical conductivity (EC_a,
dS m^{-1}); (2) inversion of EC_a to obtain electromagnetic conductivity images (EMCI) which provide the spatial distribution of
the soil electrical conductivity (σ, mS m^{-1}); (3) calibration process consisting of a regression between σ and the electrical
conductivity of the saturated soil paste extract (EC_e, dS m^{-1}), used as a proxy for soil salinity; and (4) conversion of EMCI
into salinity maps using the obtained calibration equation.

In this study, EMI surveys and soil sampling were carried out between May 2017 and October 2018 at four locations with
different salinity levels across the study area of Lezíria de Vila Franca. A previously developed regional calibration was used
for predicting EC_e from EMCI. This study aims to evaluate the potential of time-lapse EMCI and the regional calibration to
predict the spatiotemporal variability of soil salinity in the study area. The results showed that EC_e was satisfactorily predicted,
with a root mean square error (RMSE) of 3.22 dS m^{-1} in a range of 52.35 dS m^{-1} and a coefficient of determination (R^2) of
0.89. Results also showed strong concordance with a Lin's concordance correlation coefficient (CCC) of 0.93, although, EC_e
was slightly overestimated with a mean error (ME) of −1.30 dS m^{-1}. Soil salinity maps for each location revealed salinity
fluctuations related to the input of salts and water either through irrigation, precipitation or groundwater level and salinity.

Time-lapse EMCI has proven to be a valid methodology for evaluating the risk of soil salinization, and can further support the
evaluation and adoption of proper agricultural management strategies, especially in irrigated areas, where continuous
monitoring of soil salinity dynamics is required.

1 Introduction

Lezíria Grande de Vila Franca de Xira (hereafter called Lezíria de Vila Franca) is an important agricultural system of alluvial origin located by the estuary of river Tejo, northeast of Lisbon, Portugal (Fig. 1), where soil faces risk of salinization due to the marine origin of part of the sediments, tidal influence of the estuary, irrigation practices, and projected evolution of future climate with increasing temperature and decreasing precipitation. Traditional soil salinity investigations have been conducted in the study area using the electrical conductivity of a saturated soil paste extract (EC_e, dS m^{-1}) as a proxy for soil salinity. However, they were limited to few boreholes and involved soil sampling, which restricted the analysis to point information, often lacking representativeness at the field scale. In addition, borehole drilling is invasive and not feasible to conduct over large areas, given the large number of boreholes that needs to be made.

Electromagnetic induction (EMI) is widely used as a non-invasive and cost-effective solution to map soil properties over large areas. EMI measures the apparent electrical conductivity of the soil (EC_a, dS m^{-1}), which is primarily a function of soil salinity, soil texture, water content, and cation exchange capacity; however, in a saline soil, soil salinity is generally the dominant factor responsible for the spatiotemporal variability of soil EC_a. EMI surveys have been successfully used in conjunction with soil sampling to assess soil salinity through location-specific calibration between measured EC_a and soil salinity (e.g. Triantafilis et al., 2000; 2001; Corwin and Lesch, 2005; Bouksila et al., 2012). However, the ability of this method for mapping soil salinity distribution with depth is limited. This is because EMI measures EC_a, a depth-weighted average conductivity measurement, which does not represent the soil electrical conductivity (σ, mS m^{-1}) with depth. More recently, a state-of-the-art approach called electromagnetic conductivity imaging (EMCI) has permitted to obtain σ from the inversion of multi-height and/or multi sensor EC_a data (Monteiro Santos, 2004; Dafflon et al., 2013; von Hebel et al., 2014; Farzamian et al., 2015; Shanahan et al., 2015; Jadoon et al, 2015; Moghadas et al., 2017). When comparing σ with the soil properties sampled in boreholes, such as EC_e, soil water content, pH, among others, a calibration process is developed through a regression between σ and the soil properties. This way, EMCI can be converted to a map of the soil properties which show strong correlation with σ. This methodology has been applied in Lezíria de Vila Franca to study soil salinity risk (Farzamian et al., 2019; Paz et al., 2019b), and salinity and sodicity risk (Paz et al., 2019a) in which EMCI has been converted to EC_e and sodium adsorption ratio.

When repeated over a period of time, EMCI of a study area is called time-lapse EMCI, and can be used to monitor the dynamics

60   of soil salinity and other soil properties. Time-lapse EMCI has been successfully used to monitor soil water content (Huang et

al., 2017; 2018; Moghadas et al., 2017) although, to our knowledge, its potential for monitoring soil salinity has not been

previously investigated.

This study aims to evaluate the potential of time-lapse EMCI and a previously developed regional calibration to predict the

spatiotemporal variability of soil salinity, and to monitor and evaluate soil salinity dynamics in the study area. For this purpose,

65   EMI measurements and soil sampling were carried out between May 2017 and October 2018 at four locations with different

salinity levels across the study area. EMI measurements were performed with a single-coil instrument (EM38), collecting EC_a

data in the horizontal and vertical orientations and at two heights, and then inverted to obtain EMCI, which provides a vertical

distribution of σ. Finally, σ was converted to EC_e through the previously developed regional calibration. Soil samples were

collected along the EMI transects, and used for laboratory determination of EC_e. These data were used as an independent test

70   set to evaluate the ability of the regional calibration to predict the spatiotemporal variability of soil salinity, and to generate

soil salinity maps for each date of data collection.

2 Material and methods

2.1 Study area

The study was carried out in Lezíria de Vila Franca, a peninsula of alluvial origin surrounded by the rivers Tejo and Sorraia,

75   and the Tejo estuary, located 10 km northeast of Lisbon, Portugal, as shown in Fig. 1. Soils in this region have fine to very

fine texture and are classified as Fluvisols in the northern part and as Solonchaks in the southern part, according to the

Harmonized World Soil Database (Fischer et al., 2012). Climate is temperate with hot and dry summers, according to the

Köppen classification. Daily measurements of precipitation, mean temperature and reference evapotranspiration recorded

during the study period at the meteorological station represented by the blue circle in Fig. 1b, are shown in Fig. 2. Land use in

80   this area (of about 130 km²) is constituted by irrigated annual crops in the northern part and mainly by rainfed pastures in the

southern part. Irrigation is assured by an infrastructure that covers most of the area, collecting surface water at the confluence

of the two rivers. The irrigation water has low salinity with electrical conductivity typically below 0.5 dS m⁻¹ and sodium

adsorption ratio below 1 $(\text{mmol}_c\ \text{L}^{-1})^{0.5}$. The area exhibits a north-south soil salinity gradient which influences the distribution of land use types and which is probably due to the regional distribution of the marine fraction of sediments and to the saline

85 influence of the estuary on groundwater in the southern part.

Four locations were chosen in the study area, as presented in Fig. 1b, with numbers 1 to 4. Locations 1, 2, and 3 are cultivated with annual rotations of irrigated herbaceous crops in spring and annual ryegrass (*Lolium multiflorum*) in the autumn, with ploughing usually once a year. During the study years (2017 and 2018), the spring crop at location 1 was tomato drip irrigated, and at locations 2 and 3 was maize irrigated by centre pivots. Location 4 is a rainfed spontaneous pasture that hasn't been

90 ploughed at least in the last ten years. During the study period, location 1 was irrigated from 12 April to 23 July 2017 and from 30 May to 23 September 2018; location 2 was irrigated from 17 June to 11 October 2017 and from 24 May to 22 September 2018; and location 3 was irrigated from 17 May to 10 September 2017 and from 06 June to 17 September 2018. Groundwater level is shallow, as expected in an estuarine environment, and has saline characteristics. In the southern part of the study area, closer to the estuary, the depth and salinity of groundwater are influenced by tidal variation.

SOIL Open Access
Discussions EGU
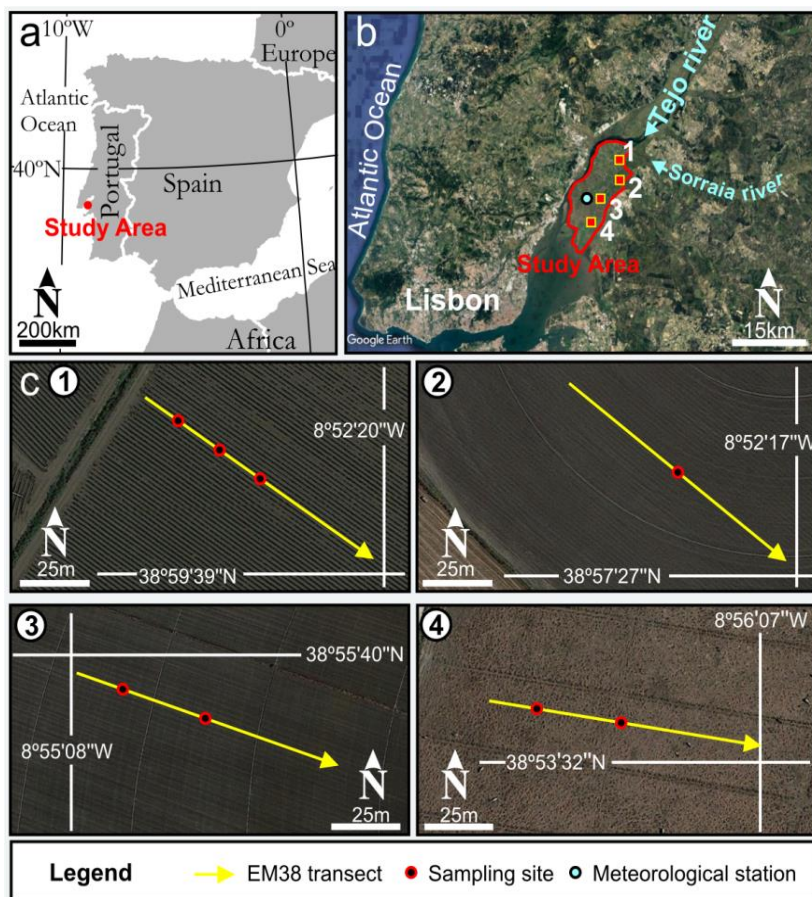
95

Figure 1: (a–b) Location of the study area in Portugal, showing the main geographical features and the four locations; (c) details of the four locations showing the EM38 transects and the soil sampling sites © Google Earth.
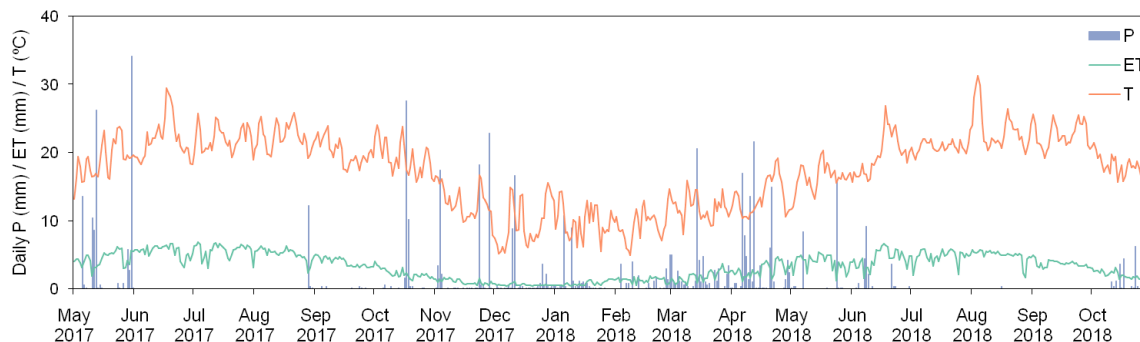
100 **Figure 2: Distribution of daily precipitation (P), reference evapotranspiration (ET) and mean temperature (T) recorded at the meteorological station located in the study area during the study period.**

2.2 Electromagnetic induction data acquisition and inversion

EMI data was acquired using the EM38 instrument (Geonics Ltd, Mississauga, Canada) on five dates at locations 1 and 4, and on six dates at locations 2 and 3, during the period of May 2017 to October 2018. Measurements on the two first dates were continuously acquired along 100 m transects using a GPS (Rikaline 6010) for registration of the position. Subsequent EMI measurements were acquired at positions 1 m apart along 20 m transects (Fig. 1c), overlapping the medium section of the 100 m transects. EC_a was collected at two heights from the soil surface (0.15 and 0.4 m) in the horizontal and vertical dipole orientations. Inversion of EC_a data to obtain σ was carried out using a 1-D laterally constrained inversion algorithm (Monteiro Santos et al., 2011). The EC_a responses of the model were calculated through forward modelling based on the full solution of the Maxwell equations (Kaufman and Keller, 1983). The subsurface model used in the inversion process consisted of a set of 1-D models distributed according to the position of the EC_a measurements. The subsurface model at each measurement position was constrained by the neighbouring models, allowing the use of the algorithm in regions characterized by high conductivity contrast. An Occam regularization (De Groot-Hedlin and Constable, 1990) based approach was used to invert the EC_a data. To run the algorithm, several parameters are selected, such as the type of inversion algorithm, the number of iterations, and the smoothing factor (λ) that controls the roughness of the model. The optimal inversion parameters for the present conditions were obtained in previous studies for the study area (Farzamian et al., 2019).

2.3 Soil sampling and laboratory analysis

Soil samples were collected at the same time of EMI surveys along the transects, as shown in Fig. 1c. At each sampling site, five soil samples were collected at 0.3 m increments to a depth of 1.35 m, as a representation of topsoil (0−0.3 m), subsurface (0.3−0.6 m), upper subsoil (0.6−0.9 m), intermediate subsoil (0.9−1.2 m), and lower subsoil (1.2−1.5 m), to monitor water content and EC_e. In the laboratory, water content was obtained using the gravimetric method, and then converted to volumetric water content (θ – m^3 m^{-3}) after bulk density determination. EC_e was measured with a conductivity meter (WTW 1C20-0211 inoLab) in the extract collected from the soil saturation paste. In this study, the soil is classified according to its EC_e level as non-saline (EC_e<2 dS m^{-1}), slightly-saline (2–4 dS m^{-1}), moderately-saline (4–8 dS m^{-1}), highly-saline (8–16 dS m^{-1}), and severely saline (>16 dS m^{-1}), according to the terminology proposed by Barrett-Lennard et al. (2008).

2.4 Prediction of EC_e from time-lapse EMCI

A regional calibration to predict EC_e from σ was previously developed for the study area resulting in the linear equation $EC_e = 0.03\sigma - 1.05$ (Farzamian et al., 2019). This calibration was termed "regional" because the equation was obtained using all EC_e and σ data collected at four locations in the study area. Farzamian et al. (2019) tested the regional and location-specific

130   calibrations, verifying that they have comparable prediction ability. However, the regional calibration can be used at any new location in the study area, within the range of measured EC_e, which makes it highly suitable for mapping and monitoring salinity in the study area. The regional calibration was based on data collected during May and June 2017 and was validated using a leave-one-out-cross-validation method with good results (RMSE = 2.54 dS m^{-1}). The detailed calibration and cross-validation procedures are described in Farzamian et al. (2019).

135   In the present study, the regional calibration was used to predict EC_e from time-lapse EMCI. The predicted EC_e and EC_e measured from soil samples, collected from July 2017 to October 2018, were used to validate the regional calibration as an independent test set. Its prediction ability was evaluated by calculating the root mean square error (RMSE), the coefficient of determination (R^2) between the measured and predicted EC_e, the Lin's concordance correlation coefficient (CCC), and the mean error (ME). The RMSE is the square root of the mean of the squared differences between the measured and predicted

140   EC_e, indicating how concentrated the data is around the linear regression. In this study we used two degrees of freedom for a more robust calculation of RMSE. The coefficient of determination (R^2) indicates how well the predicted EC_e approximate the measured EC_e. When this is 1, it means the predictions coincide with the measurements. Lin's CCC measures the agreement between the measured and predicted EC_e evaluating how close the linear regression is to the 1:1 relationship and ranges from -1 to 1, with perfect agreement at 1 (Lin, 1989). ME is the mean of all differences between the measured and predicted EC_e

145   and evaluates whether the linear regression consistently over- and underestimates the predicted EC_e. Therefore, the prediction is more precise and less biased when the RMSE and the ME are closer to zero.

4 Results and discussion

4.1 Temporal variation of measured θ and EC_e

Figure 3 shows the variation of θ and EC_e with time at the sampling site located in the middle of each transect (Fig. 1c), at

150   locations 1 to 4. At location 1, θ increases with depth and the lower subsoil (1.2–1.5 m) is permanently saturated within the

study period. In the more superficial layers until 0.9 m depth, the influence of rainfall, evapotranspiration, and irrigation is

noticeable. For instance, in the topsoil, θ peaks in January 2018 and lowers during the dry seasons, because drip irrigation

during the dry seasons has a localized effect and there is high water uptake by the crop. At location 2, unlike the other locations,

the lower subsoil is unsaturated. The influence of rainfall, evapotranspiration and irrigation is also noticeable. At locations 3

155   and 4, θ also increases with depth and the intermediate and lower subsoil layers are permanently saturated.

Regarding EC_e, at location 1 the values observed are always below 1 dS m^{-1}, except for the topsoil in September and October

2018, which is probably due to fertigation practises during the irrigation period. At location 2, EC_e generally increases with

depth. All layers show a peak in June and July 2018, probably due to fertigation practises. At location 3, EC_e reaches higher

levels than at the previous locations, exceeding 4 dS m^{-1}, which is the generally accepted threshold for the classification of

160   saline soils. Location 4 presents the highest EC_e of all locations. At the topsoil the values are below 4 dS m^{-1}, but increase

consistently with depth to about 50 dS m^{-1} in the lower subsoil. The increase of EC_e during June 2018 can be due to the

influence of saline groundwater.
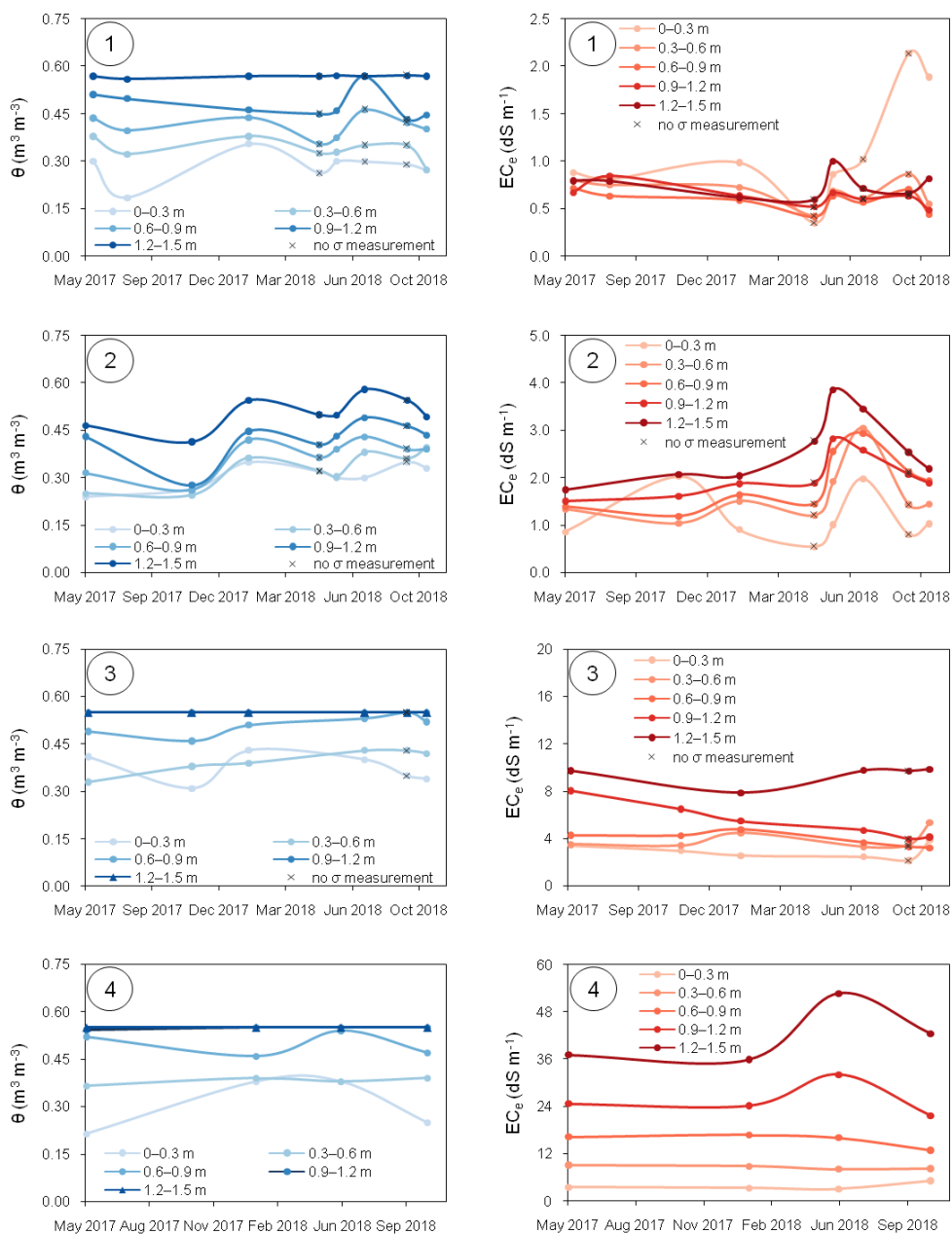
Figure 3: Volumetric water content (θ – m³ m⁻³) and electrical conductivity of the soil saturation extract (ECₑ – dS m⁻¹), in the topsoil (0–0.3 m), subsurface (0.3–0.6 m), upper subsoil (0.6–0.9 m), intermediate subsoil (0.9–1.2 m), and lower subsoil (1.2–1.5 m), measured at the sampling site located in the middle of each transect, at locations 1 to 4, during the study period.

165

4.2 Prediction of EC_e using the regional calibration

Figure 4 shows EC_e predicted with the regional calibration versus the measured EC_e and the 1:1 line, with points identified in

170   terms of date of measurement (Fig. 4a) and depth of measurement (Fig. 4b). Prediction of EC_e with the regional calibration

using data collected from July 2017 to October 2018 resulted in a RMSE of 3.22 dS m^{-1} and R^2 of 0.89, which indicates

satisfactory prediction ability, given the large range of EC_e (52.35 dS m^{-1}). The high global Lin's CCC of 0.93 shows accord

between measured and predicted EC_e. The ME is −1.30 dS m−1, indicating that the regional calibration globally overestimates

EC_e. Figure 4a and Fig. 4b show that the points are generally scattered around the 1:1 line and it is not possible to identify

175   variations depending on the date or depth of the measurement. In order to analyze the prediction ability at each location, Fig.

4c and Fig. 4d display an enlargement of the lower left part of the previous figures, displaying EC_e values below 15 dS m^{-1}.

Figure 4c and Fig. 4d show differences in the prediction ability according to the location, namely at locations 2 and 3, where

EC_e is generally overestimated. At location 2, EC_e is more overestimated in deeper soil layers (Fig. 4d) which is likely due to

a previously identified influence of clay content that consistently increases with depth at this location, while it is rather uniform

180   or declines with depth at the other locations (Farzamian et al., 2019).

The validation procedure used in this study gives lower prediction ability for the regional calibration than the previously

obtained with the leave-one-out-cross-validation (see section 2.4). This can be justified because the test set is completely

independent from the dataset used to develop the calibration. Furthermore, this test set is composed of measurements collected

over a wider period of time (18 months). During this period, soil properties, which are also known to influence σ, such as θ,

185   change (as shown in Fig. 3), which introduces larger variability in the measurements. However, and given the large range of

EC_e (52.35 dS m^{-1}), a RMSE of 3.22 dS m^{-1} is acceptable for this type of non-invasive and indirect method. The regional

calibration could be further developed by including measurements taken over a longer period of time in the calibration process,

in order to include a wider range of variation of soil properties.

190
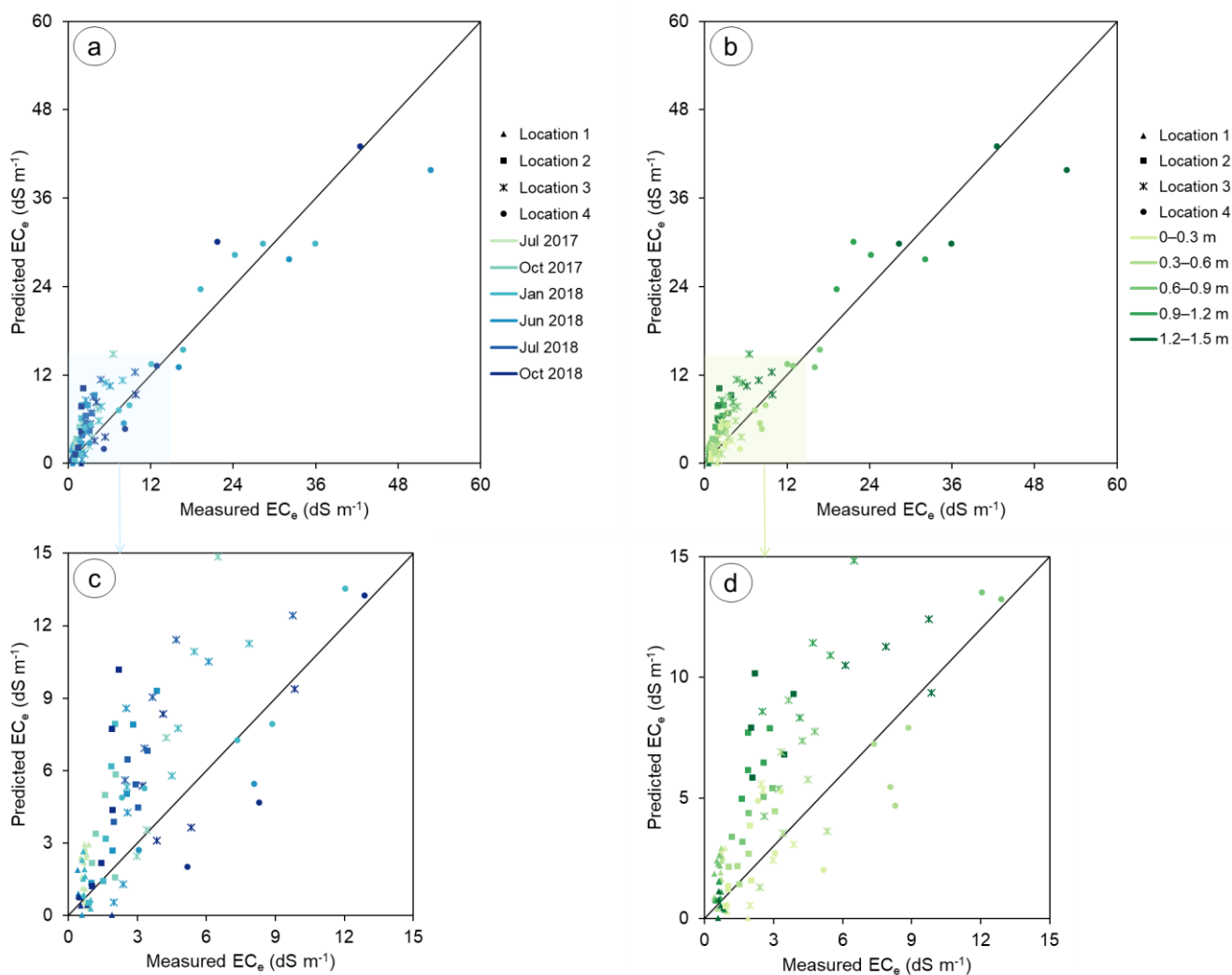
Figure 4: Plots of predicted EC_e versus measured EC_e and the 1:1 line, obtained for locations 1 to 4, identified in terms of date of measurement (a) and depth of measurement (b). Plots (c) and (d) show enlargements of the lower left part of plots (a) and (b), respectively.

195 **4.3 Spatiotemporal mapping of soil salinity from time-lapse EMCI**

Figure 5 shows the soil salinity maps (EC_e predicted using the regional calibration) at locations 1 to 4 for each date of the EMI surveys, categorized into 6 salinity classes, ranging from non-saline to severely-saline. The measured EC_e and the groundwater level at the sampling site located in the middle of each EMI transect are also shown.
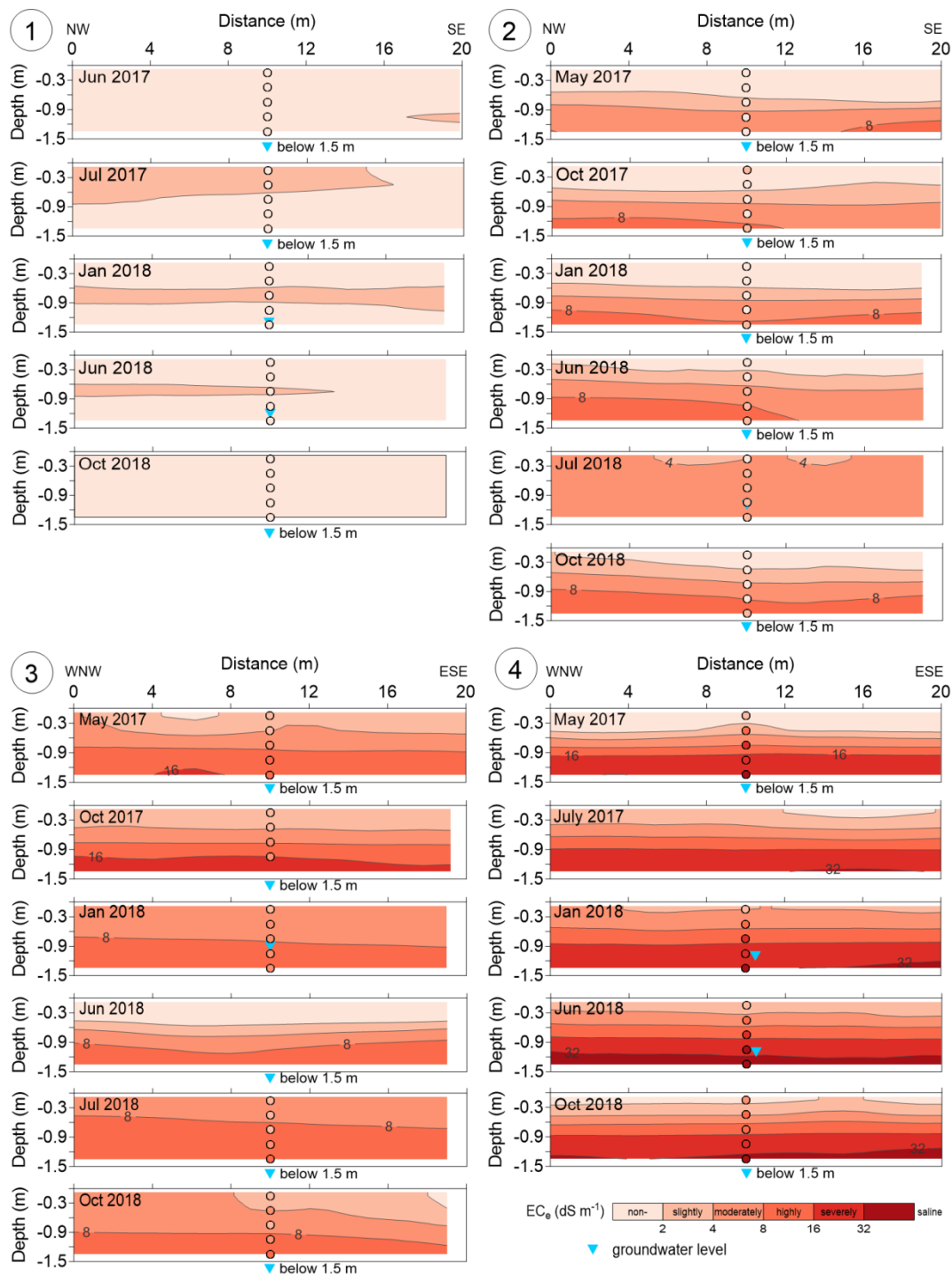
Figure 5: Maps of soil salinity (predicted EC_e) for locations 1 to 4, with representation of measured EC_e (in circles) and groundwater level (blue triangles) at the sampling sites located in the middle of each transect. Note that in June 2018 at location 3 and in July 2017 at location 4 there was no soil sampling.

200

13

205   The salinity maps for location 1 show that the soil is generally non-saline, with slightly saline zones in all dates except for
October 2018. These saline zones occur in the top soil layers until 0.9 m depth (topsoil, subsurface and upper subsoil), and
represent an overestimation of the soil salinity when compared to the measured EC_e of the sampling point (which is invariably
non-saline). This overestimation tendency is in agreement with Fig. 4d, where the very low range of spatiotemporal variations
of soil salinity at this location can also be observed. In such conditions, other soil properties, such as θ, dominate the small
210   variations of σ, and therefore the ability to predict salinity from σ at this location was reduced. Our previous studies with both
location-specific and regional calibrations tested at this location showed similar results (Farzamian et al., 2019).

At location 2 the salinity maps show an increase of salinity with depth from non-saline at the topsoil to highly-saline in the
lower subsoil, with exception of July 2018, where the entire soil profile is moderately saline. The increase of soil salinity in
upper soil layers in July 2018 can be attributed to fertigation practices for the maize cultivation that introduced salts into the
215   soil profile. The salinity maps also show the overestimation of salinity occurring mainly at deeper soil layers, which agrees
with the results presented in Fig. 4d and discussed in section 4.2.

At location 3 soil salinity is well predicted in May 2017 but tends to be slightly overestimated in the remaining dates, especially
in July 2018. The salinity maps show that salinity increases with depth reaching severely-saline in May 2017 and
October 2017. This can be due to the influence of the saline groundwater (as seen in Fig. 3, the intermediate and lower subsoil
220   layers are permanently saturated). The groundwater level is above 1.5 m in January 2018, although the salinity of the deeper
soil layers (>0.9 m) decreases compared to May and October 2017, which could be due to washing of the profile by rainfall.

At location 4 the trend of increasing salinity with depth is accurate in all dates, but it tends to be slightly underestimated. The
salinity maps show that salinity increases from non-saline in topsoil to severely-saline in lower subsoil. This is probably related
to the saline groundwater level above 1.5 m. During the dry period of the year, salinity of the lower subsoil reaches the highest
225   values (June 2018).

Comparison of the salinity maps between locations confirms the previously known north-south soil salinity spatial gradient of
the study area, that is, from location 1 to 4, soil salinity generally increases. Soil salinity dynamics at each location reveals
fluctuations in time related to the input of salts and water either through irrigation, precipitation or groundwater level and

salinity. Location 1 tends to have non-saline characteristics, which can be attributed to good quality irrigation water and to the

230   fact that this location is far from the estuary, making it less prone to the presence of saline groundwater. At locations 2 and 3,

the salinity maps show an increase of soil salinity in the upper layers during the dry season (when irrigation occurs), which

decreases in the following months with increased rainfall (Fig. 2). At the rainfed location 4, it is also visible an increment of

salinity along the entire profile during the dry season. This is likely due to the influence of the saline groundwater and capillary

rise along the profile.

235   **5 Conclusions**

In this study, EMI and soil sampling data collected between May 2017 and October 2018 were used, together with a previously

developed regional calibration, to predict the spatiotemporal variability of soil salinity. This procedure allowed to further

validate the regional calibration with an independent test set. This validation resulted in lower prediction ability than that

previously resulting from cross-validation, not only because the test set was independent, but also because it was collected

240   over a wider period of time, during which the variation of soil properties is larger. The validation used in this study resulted in

a RMSE of 3.22 dS m^{-1}, which is acceptable given the large range of EC$_e$ (52.35 dS m^{-1}). As a result, the regional calibration

approach still stands as an expeditious method to predict soil salinity in the study area over time. The regional calibration could

be further developed by studying new locations across the study area in order to include a wider range of variation of soil

properties. Also, a longer period of observation could further improve the regional calibration. Furthermore, the influence of

245   static soil properties (i.e., that do not vary in time), such as clay content, could be tackled with the use of maps of the variation

of soil salinity between two consecutive dates, which allows removing the static effect in the EMCIs.

Relatively to the inversion process, in the absence of a time-lapse inversion algorithm, EC$_a$ data was inverted independently.

This method can distort the inversion results, since the reference model and a priori information are not considered. Further

research involves time-lapse inversion algorithms that are being developed to invert data collected with EMI sensors, which

250   can generate EMCIs of higher precision.

The methodology used in this study allowed the creation of soil salinity maps displaying the spatiotemporal patterns of soil

salinity at four locations in the study area. The salinity maps reveal fluctuations in time related to the input of salts and water

either through irrigation, precipitation or groundwater level and salinity. In a regional perspective, soil salinity dynamics in the study area may be explained by a combination of spatial distribution of the marine fraction of soil, with irrigation practices in the study area and saline groundwater in the southern part. Continuous monitoring of salinity in the study area, along with detailed data collection about irrigation, precipitation, evapotranspiration, leaching, groundwater flow, and tides, can be helpful to further study soil salinity dynamics.

Time-lapse EMCI has proven to be a valid methodology for evaluating risk of soil salinization, and can further support the evaluation and adoption of proper agricultural management strategies, especially in irrigated areas, where continuous monitoring of soil salinity dynamics is required.

Acknowledgements

265

The authors are grateful to the Associação de Beneficiários da Lezíria Grande de Vila Franca de Xira and to Manuel Fernandes and Fernando Pires from INIAV for field assistance.

270

SOIL
Discussions

Open Access

EGU

References

Barrett-Lennard, E. G., Bennett, S. J., and Colmer, T. D.: Standardising the terminology for describing the level of salinity in soils. In: Proceedings of the 2nd international salinity forum: Salinity, water and society global issues, local action,

275   Adelaide, SA, Australia, 31 Mar.–3 Apr. 2008. Geological Society of Australia, Hornsby, NSW, Australia, 2008.

Bouksila, F., Persson, M., Bahri, A., and Berndtsson, R.: Electromagnetic induction prediction of soil salinity and groundwater properties in a Tunisian Saharan oasis. Hydrol. Sci. J., 57, 1473–1486, https://doi.org/10.1080/02626667.2012.717701, 2012.

Corwin, D.L. and Lesch, S.M.: Characterizing soil spatial variability with apparent soil electrical conductivity: I. Survey

280   protocols. Comp. Elec. Agri. Appl. Apparent Soil Elec. Conductivity Precis. Agri., 46, 103–133, https://doi.org/10.1016/j.compag.2004.11.002, 2005.

Dafflon, B., Hubbard, S., Ulrich, C., and Peterson, J.E.: Electrical conductivity imaging of active layer and permafrost in an arctic ecosystem, through advanced inversion of electromagnetic induction data. Vadose Zone J., 12, https://doi.org/10.2136/vzj2012.0161, 2013.

285   De Groot-Hedlin, C. and Constable, S.C.: Occam's inversion to generate smooth, two dimensional models from magnetotelluric data. Geophysics, 55, 1613–1624, https://doi.org/10.1190/1.1442813, 1990.

Farzamian, M., Monteiro Santos, F. A., and Khalil, A.M.: Application of EM38 and ERT methods in estimation of saturated hydraulic conductivity in unsaturated soil. J. Appl. Geophys., 112, 175–189, https://doi.org/10.1016/j.jappgeo.2014.11.016, 2015.

290   Farzamian, M., Paz, M.C., Paz, A.M., Castanheira, N.L., Gonçalves, M.C., Santos, F.A.M., and Triantafilis, J.: Mapping soil salinity using electromagnetic conductivity imaging-a comparison of regional and location-specific calibrations. Land Degrad. Dev., 30, 1393–1406, https://doi.org/10.1002/ldr.3317, 2019.

Fischer, G., Nachtergaele, F.O., Prieler, S., Teixeira, E., Toth, G., van Velthuizen, H., Verelst, L., and Wiberg, D.: Global Agro-ecological Zones (GAEZ v3.0)-Model Documentation [WWW Document]. URL http://www.fao.org/soils-

295   portal/soil-survey/soil-maps-and-databases/harmonized-world-soil-database-v12/en/ (accessed 12.17.18), 2012.

Huang, J., Purushothaman, R., McBratney, A., and Bramley, H.: Soil water extraction monitored per plot across a field experiment using repeated electromagnetic induction surveys. Soil Syst., 2(1), 11, https://doi.org/10.3390/soilsystems2010011, 2018.

Huang, J., Scudiero, E., Clary, W., Corwin, D. L., and Triantafilis, J.: Time-lapse monitoring of soil water content using electromagnetic conductivity imaging. Soil Use Manage., 33, https://doi.org/10.1111/sum.12261, 2017.

Jadoon, K.Z., Moghadas, D., Jadoon, A., Missimer, T.M., Al-Mashharawi, S.K., and McCabe, M.F.: Estimation of soil salinity in a drip irrigation system by using joint inversion of multicoil electromagnetic induction measurements. Water Resour. Res., 51, 3490–3504, https://doi.org/10.1002/2014WR016245, 2015.

Kaufman, A.A. and Keller, G.V.: Frequency and transient soundings. Methods in Geochemistry and Geophysics, 16. Elsevier, New York, https://doi.org/10.1111/j.1365-246X.1984.tb02230.x, 1983.

Lin, L. I. K.: A concordance correlation coefficient to evaluate reproducibility. Biometrics, 45, 255–268, https://doi.org/10.2136/sssaj1998.03615995006200010030x, 1989.

Moghadas, D., Jadoon, K.Z., and McCabe., M.F.: Spatiotemporal monitoring of soil water content profiles in an irrigated field using probabilistic inversion of time-lapse EMI data. Adv. Water Resour., 110, 238–248, https://doi.org/10.1016/j.advwatres.2017.10.019, 2017.

Monteiro Santos, F.A.: 1-D laterally constrained inversion of EM34 profiling data. J. Appl. Geophys., 56, 123–134, https://doi.org/10.1016/j.jappgeo.2004.04.005, 2004.

Monteiro Santos, F.A., Triantafilis, J., and Bruzgulis, K.: A spatially constrained 1D inversion algorithm for quasi-3D conductivity imaging: application to DUALEM-421 data collected in a riverine plain. Geophysics, 76, B43–B53, https://doi.org/10.1190/1.3537834., 2011.

Paz, A., Castanheira., N., Farzamian, M., Paz, M.C., Gonçalves, M., Monteiro Santos, F., and Triantafilis, J.: Prediction of soil salinity and sodicity using electromagnetic conductivity imaging. Geoderma, https://doi.org/10.1016/j.geoderma.2019.114086, *in press*, 2019a.

Paz, M.C., Farzamian, M., Monteiro Santos, F., Gonçalves, M.C., Paz, A.M., Castanheira., N.L., and Triantafilis, J.: Potential

320   to map soil salinity using inversion modelling of EM38 sensor data. First Break, 37(6), 35–39, doi:10.3997/1365-2397.2019019, 2019b.

Shanahan, P.W., Binley, A., Whalley, W.R., and Watts., C.W.: The use of electromagnetic induction to monitor changes in soil moisture profiles beneath different wheat genotypes. Soil Sci. Soc. Am. J., 79, 459–466, https://doi.org/10.2136/sssaj2014.09.0360, 2015.

325   Triantafilis. J., Laslett, G.M., and McBratney, A.B.: Calibrating an electromagnetic induction instrument to measure salinity in soil under irrigated cotton. Soil Sci. Soc. Am. J., 64, 1008-1017, https://doi.org/10.2136/sssaj2000.6431009x, 2000.

Triantafilis, J., Odeh, I.O.A.V., and McBratney, A.B.: Five geostatistical methods to predict soil salinity from electromagnetic induction data across irrigated cotton. Soil Sci. Soc. Am. J., 65, 869-978, https://doi.org/10.2136/sssaj2001.653869x, 2001.

Triantafilis, J. and Monteiro Santos, F.A.: 2-dimensional soil and vadose zone representation using an EM38 and EM34 and a

330   laterally constrained inversion model. Aust. J. Soil Res., 47, 809–820, https://doi.org/10.1071/SR09013, 2009.

von Hebel, C., Rudolph, S., Mester, A., Huisman, J.A., Kumbhar, P., Vereecken, H., and van der Kruk, J.: Three-dimensional imaging of subsurface structural patterns using quantitative large-scale multi-configuration electromagnetic induction data. Water Resour. Res., 50, 2732–2748, https://doi.org/10.1002/2013wr014864, 2014.